Low-symmetry two-dimensional BNP_2 and C_2SiS structures with high and anisotropic carrier mobilities

Shixin Song [1], Jie Guan [1,*], and David Tománek [2,†]

[1]*School of Physics, Southeast University, Nanjing, 211189, People's Republic of China*
[2]*Physics and Astronomy Department, Michigan State University, East Lansing, Michigan 48824, USA*

We study the stability and electronic structure of previously unexplored two-dimensional (2D) ternary compounds BNP_2 and C_2SiS. Using *ab initio* density functional theory, we have identified four stable allotropes of each ternary compound and confirmed their stability by calculated phonon spectra and molecular dynamics simulations. Whereas all BNP_2 allotropes are semiconducting, we find C_2SiS, depending on the allotrope, to be semiconducting or semimetallic. The fundamental band gaps of the semiconducting allotropes we study range from 1.4 eV to 2.2 eV at the HSE06 level and display carrier mobilities as high as 1.5×10^5 cm^2 V^{-1} s^{-1}. Such high mobilities are quite uncommon in semiconductors with so wide band gaps. Structural ridges in the geometry of all allotropes cause a high anisotropy in their mechanical and transport properties, promising a wide range of applications in electronics and optoelectronics.

I. INTRODUCTION

Two-dimensional (2D) materials have intrigued researchers around the world since the successful mechanical exfoliation of graphene [1]. Even though graphene remains unsurpassed in terms of high charge carrier mobility, the vanishing band gap in the pristine material precludes its use from semiconducting circuitry [2,3]. Other 2D materials including transition metal dichalchogenides (TMDs) such as MoS_2 have sizable band gaps but are not as useful due to their low carrier mobility [4,5]. Phosphorene, a monolayer of black phosphorus, combines high and anisotropic carrier mobility with a sizable and tunable band gap [6–8] but is unstable under ambient conditions [9]. In spite of significant efforts to improve the performance of 2D materials in semiconducting devices, the progress has been moderate. There is a need to find new 2D semiconductors with substantial band gaps and high carrier mobilities.

Phosphorus carbide (PC), a recently proposed 2D material, has been predicted to be stable [10] and to display promising electronic behavior including high carrier mobility [11]. Of the stable allotropes, the semiconducting α_1-PC phase, also called black phosphorus carbide (*b*-PC), has been successfully synthesized. It shows a high field-effect mobility $\mu =$ 1995 cm^2 V^{-1} s^{-1} of holes at room temperature [12], good infrared response [13], and tunable anisotropic plasmonic performance [14]. The narrow band gap, however, limits the performance of PC-based field-effect transistors (FETs) due to a relatively low ON/OFF ratio [12]. Experimental data for 2D GeP [15], another low-symmetry IV-V compound with strongly anisotropic conductance, indicate a high field-effect ON/OFF ratio $\approx 1 \times 10^4$ but a low carrier mobility

$\mu = 0.35$ cm^2 V^{-1} s^{-1}. Theoretical explorations have been extended to other 2D IV-V compounds, which are not isoelectronic to PC. These include germanium triphosphide [16] GeP_3, tin triphosphide [17] SnP_3, and phosphorus hexacarbide [18] PC_6. However, all these systems have narrow band gaps similar to α_1-PC and share a hexagonal honeycomb lattice structure and thus a weak transport anisotropy. 2D structures with a substantial band gap, high carrier mobility, and strong in-layer anisotropy are still missing.

In search of such 2D materials inspired by anisotropic 2D PC structures, we have applied an effective design strategy known as "isoelectronic substitution." This process involves substituting certain elements in the structure by their neighbors in the periodic table yet keeping the total valence electron count unchanged. This approach, which has been successfully applied in both 3D and 2D systems, allows us to change physical and chemical properties of the system without drastically changing the structure. In this way, the diamond structure of bulk silicon with a diatomic unit cell can be changed to the isoelectronic Si_3AlP, when one Si atom is substituted by Al and the other by P in every other unit cell, thus significantly increasing light absorption in the visible region [19]. In semimetallic 2D graphene with a diatomic basis, substituting one C atom by B and the other by N forms the *h*-BN structure, a wide-gap insulator. In a similar way, substituting every other atom in phosphorene by Si and S atoms results in the 2D SiS structure [20,21]. The same isoelectronic substitution in 2D group V systems leads to 2D group IV-VI compounds including GeS, GeSe, and SnS with a lower symmetry and a wide range of physical properties [22–25].

In this study, we propose isoelectronic substitution in 2D structures of phosphorus carbide that leads to previously unknown ternary compounds BNP_2 and C_2SiS. Our *ab initio* density functional calculations identify four stable allotropes of each compound that share the 2D geometry with PC. Calculated phonon spectra and *ab initio* molecular
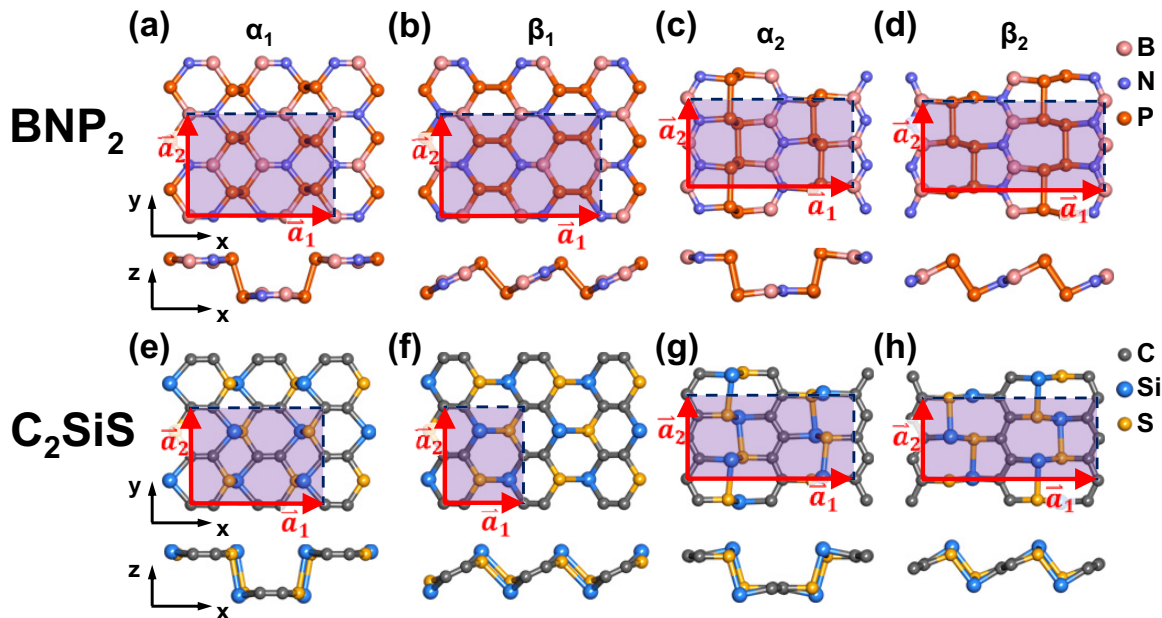
*guanjie@seu.edu.cn
†tomanek@msu.edu

FIG. 1. Ball-and-stick models of relaxed monolayer structures of (a) α_1, (b) β_1, (c) α_2 and (d) β_2 allotropes of BNP_2, and (e) α_1, (f) β_1, (g) α_2 and (h) β_2 allotropes of C_2SiS in top and side view. The lattice vectors are indicated by red arrows.

dynamics (MD) simulations confirm the stability of each of these allotropes. Due to structural ridges in the geometry, all allotropes considered exhibit a significant anisotropy in the elastic response. Electronic structure calculations indicate that α_1 and β_1 phases of C_2SiS, as well as all four BNP_2 allotropes, are semiconductors with a wide range of band gap values. Carrier mobility calculations show that most of the semiconducting allotropes exhibit high and strongly anisotropic carrier mobilities. The remaining α_2-C_2SiS and β_2-C_2SiS allotropes were found to be semimetallic, displaying an elliptically distorted Dirac cone in their band structure caused by their structural anisotropy.

II. COMPUTATIONAL TECHNIQUES

We have used *ab initio* density functional theory (DFT), as implemented in the VASP code [26–28], throughout the study. We applied periodic boundary conditions, with 2D structures separated by a vacuum region in excess of 20 Å. The reciprocal space was sampled by a fine grid [29] of $8 \times 6 \times 1$ k points in the Brillouin zone of eight-atom unit cells or its equivalent in supercells. We used projector-augmented-wave (PAW) pseudopotentials [30] and the Perdew-Burke-Ernzerhof (PBE) [31] exchange-correlation functionals. Selective band structure calculations were performed using the hybrid HSE06 functional [32,33] with the default mixing parameter $\alpha = 0.25$. We utilized the DFT-D2 [34] method to represent van der Waals (vdW) corrections to the total energy. We used a cutoff energy of 500 eV for the plane-wave basis set and considered the electronic structure to be converged once the total energy difference between subsequent electronic structure iterations would not exceed 10^{-5} eV. All geometries were optimized using the conjugate-gradient method [35], until none of the residual Hellmann-Feynman forces exceeded 10^{-2} eV/Å. The phonon calculations were carried out using

the density functional perturbation theory [36–38], as implemented in the PHONOPY code [39]. The system dynamics was studied using canonical *ab initio* MD simulations with 3 fs time steps. Our results are for supercells containing more than 100 atoms, which were kept at temperatures of 300 K, 500 K, or 1000 K for periods exceeding 15 ps.

III. RESULTS AND DISCUSSION

A. Structure of BNP_2 and C_2SiS 2D allotropes

As introduced above, the 2D compounds BNP_2 and C_2SiS are isoelectronic to previously reported PC monolayer structures [10]. We have identified four 2D allotropes, called α_1, β_1, α_2, and β_2, for each of the systems. The most stable structures of each allotrope are shown in Fig. 1. All atoms are threefold coordinated, causing a coexistence of sp^2 and sp^3 bonding and leading to structural ridges in the geometry of all allotropes. When viewed from the side, the α allotropes have an armchair profile, whereas the β allotropes have a zigzag profile. With the exception of β_1-C_2SiS with eight atoms in the unit cell, all allotropes have rectangular unit cells containing sixteen atoms. Additional metastable structures with different atomic arrangements in the unit cell are discussed in the Appendix.

As seen in Fig. 1, the optimized α_1 and β_1 allotropes of BNP_2 structures consist of isolated P-P and B-N dimers forming a 2D hexagonal structure. Since the orientation of the B-N dimers alternates in the plane of the system, there is no net dipole moment in the system. P atoms prefer the sp^3 configuration with a lone electron pair, whereas B and N atoms prefer the sp^2 configuration in all BNP_2 allotropes. The α_1 and β_1 allotropes represent two equivalent ways to achieve optimum configuration with the same topology, in analogy to black and blue phosphorene [40].

TABLE I. Calculated equilibrium properties of BNP$_2$ and C$_2$SiS 2D allotropes.

	BNP$_2$				C$_2$SiS			
	α_1	β_1	α_2	β_2	α_1	β_1	α_2	β_2
$|\vec{a}_1|$ (Å)[a]	8.50	9.39	9.44	10.44	8.07	4.75	9.83	10.61
$|\vec{a}_2|$ (Å)[a]	5.97	5.97	5.14	5.14	5.87	5.86	5.03	5.03
$d_{P\text{-}P}$ (Å)[b]	2.25	2.25	2.27[h]	2.27[h]				
			2.24[i]	2.23[i]				
$d_{P\text{-}N}$ (Å)[b]	1.78	1.78	1.79	1.79				
$d_{P\text{-}B}$ (Å)[b]	1.94	1.94	1.95	1.95				
$d_{B\text{-}N}$ (Å)[b]	1.40	1.40	1.46	1.46				
$d_{Si\text{-}S}$ (Å)[b]					2.49	2.46	2.41[h]	2.40[h]
							2.35[i]	2.35[i]
$d_{C\text{-}S}$ (Å)[b]					1.77	1.77	1.77	1.77
$d_{C\text{-}Si}$ (Å)[b]					1.94	1.94	1.95	1.95
$d_{C\text{-}C}$ (Å)[b]					1.36	1.36	1.42	1.42
E_{coh} (eV/atom)[c]	4.74	4.74	4.98	4.98	5.25	5.26	5.54	5.54
E_{form} (eV/atom)[d]	−0.01	−0.01	−0.25	−0.24	0.68	0.68	0.39	0.39
c_{11} (N/m)[e]	7.17	40.59	10.24	57.53	6.42	33.79	14.89	53.35
c_{22} (N/m)[e]	156.02	144.13	189.59	173.68	145.94	124.02	199.72	185.35
$E_{g\text{-}PBE}$ (eV)[f]	0.52	0.80	1.39	1.26	0.71	0.70	0.00	0.00
$E_{g\text{-}HSE06}$ (eV)[g]	1.38	1.69	2.15	2.06	1.57	1.40	0.00	0.00

[a]$|\vec{a}_1|$ and $|\vec{a}_2|$ are the in-plane lattice constants defined in Fig. 1.
[b]d is the equilibrium bond length between the respective species.
[c]E_{coh} is the cohesive energy per average atom with respect to isolated atoms.
[d]E_{form} is the formation energy per average atom with respect to elemental structures.
[e]c_{11} (c_{22}) are the 2D elastic constants along the x (y) direction.
[f]$E_{g\text{-}PBE}$ is the band gap value at the DFT-PBE level.
[g]$E_{g\text{-}HSE06}$ is the band gap value at the DFT-HSE06 level.
[h]Length of bonds within the structural plane.
[i]Length of bonds out of the structural plane.

The α_2 and β_2 allotropes of BNP$_2$ contain alternating chains of P and BN along the y direction. The mismatch between the equilibrium P-P and B-N bond lengths leads to the formation of pentagon-heptagon pairs instead of hexagons.

The structure of all 2D allotropes of C$_2$SiS closely resembles that of BNP$_2$ due to the coexistence of sp^2-bonded C atoms and sp^3-bonded Si and S atoms. Similar to BNP$_2$, the α_1 and β_1 allotropes of C$_2$SiS contain isolated Si-S and C-C dimers. Also in this case, there are two distinguishable, topologically equivalent geometries. Even though the polar Si-S bonds are out of plane in this compound, their alternating orientation eliminates a net dipole moment. The α_2 and β_2 allotropes of C$_2$SiS, analogous to those of BNP$_2$, contain alternating C and SiS chains along the y direction. Bond length mismatch leads to a preferential formation of pentagon-heptagon pairs in the layer.

A summary of the structural characteristics and the cohesive energy of all these allotropes is presented in Table I. In the BNP$_2$ system, the B-N dimers in α_1 and β_1 allotropes are connected by typical double bonds with $d_{BN} \approx 1.40$ Å, close to the 1.403 Å value in amino borane [41]. The bond length of the B-N chains in α_2 and β_2 allotropes is slightly longer, at about 1.46 Å, close to the 1.45 Å value in 2D h-BN [42]. These results are consistent with the sp^2 configuration of B and N atoms in 2D BNP$_2$.

We find similar structural characteristics in the C$_2$SiS system. As expected for sp^2-bonded C atoms, the C-C bond

lengths are comparable to the double bonds in ethylene and the conjugated bonds in benzene or graphene. The length of all the other single bonds appears rather insensitive to the structure.

It is also noteworthy that P-N bonds are slightly shorter than P-B bonds in BNP$_2$ due to the smaller atomic radius of the more electronegative element. The same is true, for the same reason, with the C-S bonds that are slightly shorter than C-Si bonds in C$_2$SiS allotropes.

For the sake of easy comparison, we define the cohesive energy E_{coh} of an "average" atom by dividing the total atomization energy by the total number of atoms. Our results for E_{coh} are listed in Table I. We found that for both BNP$_2$ and C$_2$SiS, α and β allotropes with the same index are almost equally stable. Our results also indicate that for both BNP$_2$ and C$_2$SiS, α_2 and β_2 allotropes are energetically more stable than α_1 and β_1 allotropes by $\Delta E_{coh} \approx 0.2$–0.3 eV/atom. We find the C$_2$SiS structures to be generally more stable than BNP$_2$ structures. The listed values of $E_{coh} \approx 5$ eV/atom here are comparable to cohesive energies found in PC monolayers [10].

We have further confirmed the stability of each allotrope by calculating the phonon spectra and by performing *ab initio* MD simulations. Details of all these calculations are presented in the Appendix.

We also calculated the formation energy per 'average atom' E_{form} to investigate the relative stability of the ternary allotropes comparing with respect to their elemental

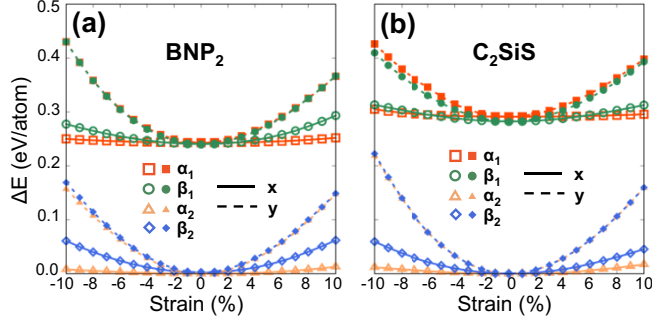FIG. 2. Effect of uniaxial in-layer strain on the relative binding energy ΔE in monolayers of (a) BNP_2 and (b) C_2SiS. Results for different allotropes are distinguished by color and symbols. Results for strain along the x direction are shown by solid lines and for strain along the y direction by dashed lines.

components. We defined E_{form} as

$$E_{form}(X_l Y_m Z_n) = E(X_l Y_m Z_n) \\ - \frac{l \cdot E(X) + m \cdot E(Y) + n \cdot E(Z)}{l + m + n}, \quad (1)$$

where $E(X_l Y_m Z_n)$, $E(X)$, $E(Y)$, $E(Z)$ are the respective total energies per average atom of the $X_l Y_m Z_n$ compound and the elemental structures of X, Y, and Z. In the particular case of 2D BNP_2 and C_2SiS structures, the elemental structures we consider are bulk boron, gas of N_2 molecules, phosphorene, graphene, bulk silicon, and bulk sulfur. The results of E_{form} for all the allotropes are listed in Table I. $E_{form} > 0$ indicates instability and possibility of exothermic decomposition, whereas $E_{form} < 0$ indicates stability.

Our results for E_{form} in Table I indicate that all BNP_2 allotropes are stable and will not decompose below ≈ 1000 K, at which point bonds may be broken. The values of E_{form} for C_2SiS allotropes considered here are positive but rather small. The values $E_{form} = 0.68$ eV/atom for the α_1 and β_1 phases and $E_{form} = 0.39$ eV/atom for the α_2 and β_2 phases are an order of magnitude smaller than cohesive energies and comparable to $E_{form} = 0.54$ eV/atom found in 2D-PC [10]. Structural changes would require overcoming a significant activation barrier associated with breaking bonds and protect C_2SiS allotropes from structural changes at room temperature. As mentioned above, interatomic bonds may break and structural changes may become possible at extremely high temperatures of ≈ 1000 K. We find these estimates confirmed by our MD simulation results presented in the Appendix.

B. Anisotropic in-plane stiffness of 2D BNP_2 and C_2SiS allotropes

To investigate the elastic response of the 2D ternary structures, we subjected all allotropes in this study to in-layer uniaxial strain along the x and y direction and display differences ΔE_{coh} of the average binding energy with respect to the most stable allotrope in Fig. 2. The presence of structural ridges renders all allotropes much softer along the x direction normal to the ridge direction. The α allotropes of both BNP_2 and C_2SiS are particularly soft along the x direction, with $\Delta E \lesssim 18$ meV/atom when subjected to $\leqslant 10\%$ compressive or

tensile strain. The 2D elastic moduli [43] c_{ii} along the x and y direction, obtained using these calculations, are summarized in Table I. For the semiconducting allotropes, these values play an important role in carrier mobilities.

C. Electronic structure of BNP_2 2D allotropes

Results of our DFT calculations for the electronic structure of BNP_2 monolayers are presented in Fig. 3. Our DFT-PBE results show all four allotropes to be semiconductors. The fundamental band gap is direct in α_1-BNP_2 and indirect in all the other BNP_2 allotropes. Band gap values E_g based on DFT-PBE Kohn-Sham energies, ranging from 0.52 eV to 1.39 eV, are listed in Table I. We should note here that the interpretation of Kohn-Sham eigenvalues as self-energies is strictly incorrect and that DFT-based band gaps are typically underestimated. We find this to be the case when comparing band gap values based on DFT-PBE and the hybrid DFT-HSE06 functional in Table I. As seen when comparing band structure results based on DFT-PBE, given by the solid lines in Fig. 3, and DFT-HSE06, shown by the red dashed lines, the main difference is the opening of the fundamental band gap in DFT-HSE06, whereas the band dispersion is unaffected. We also present the total electronic density of states (DOS) and its projection onto the different species next to the band structure plots.

Contour plots of the projected DOS (PDOS) of all BNP_2 allotropes at the valence band maximum (VBM) and conduction band minimum (CBM) are shown in Fig. 3, with the contributions to VBM and CBM distinguished by color. We find the character of the VBM to be dominated by the lone-pair states of the sp^3 hybridized P atoms in all BNP_2 allotropes. The character of the CBM is very different. The dominant contribution in α_1 and β_1 allotropes of BNP_2 comes from out-of-plane p orbitals of sp^2 hybridized B and N atoms. In the α_2 and β_2 allotropes, p orbitals of all the atoms contribute to the CBM character.

We also observe an unusually flat band in the band structure of α_2 and β_2 allotropes of BNP_2 at the top of the valence region, along the Γ-X line. To further explore the origin of this flat band, we show 2D contour plots of the dispersion within the top valence and bottom conduction bands in Fig. 4.

In both allotropes, the CBM energy minimum occurs at the Γ point and the band dispersion around is almost isotropic and free-electron-like. In contrast, the VBM is displaced from the Γ point in the direction towards X for both allotropes. Whereas the band dispersion is almost flat along the x direction, it is significantly higher along the y direction near the VBM, indicating a significant anisotropy in the carrier effective mass. As seen in Figs. 3(b) and 3(d), this is caused at the VBM by a larger separation and lower hybridization between the P lone pair states along the x direction than along the y direction.

D. Electronic structure of C_2SiS 2D allotropes

Results of our DFT calculations for the electronic structure of C_2SiS monolayers are presented in Fig. 5. Our findings indicate that only the α_1 and the β_1 allotropes are semiconducting, whereas the α_2 and β_2 allotropes are semimetallic.
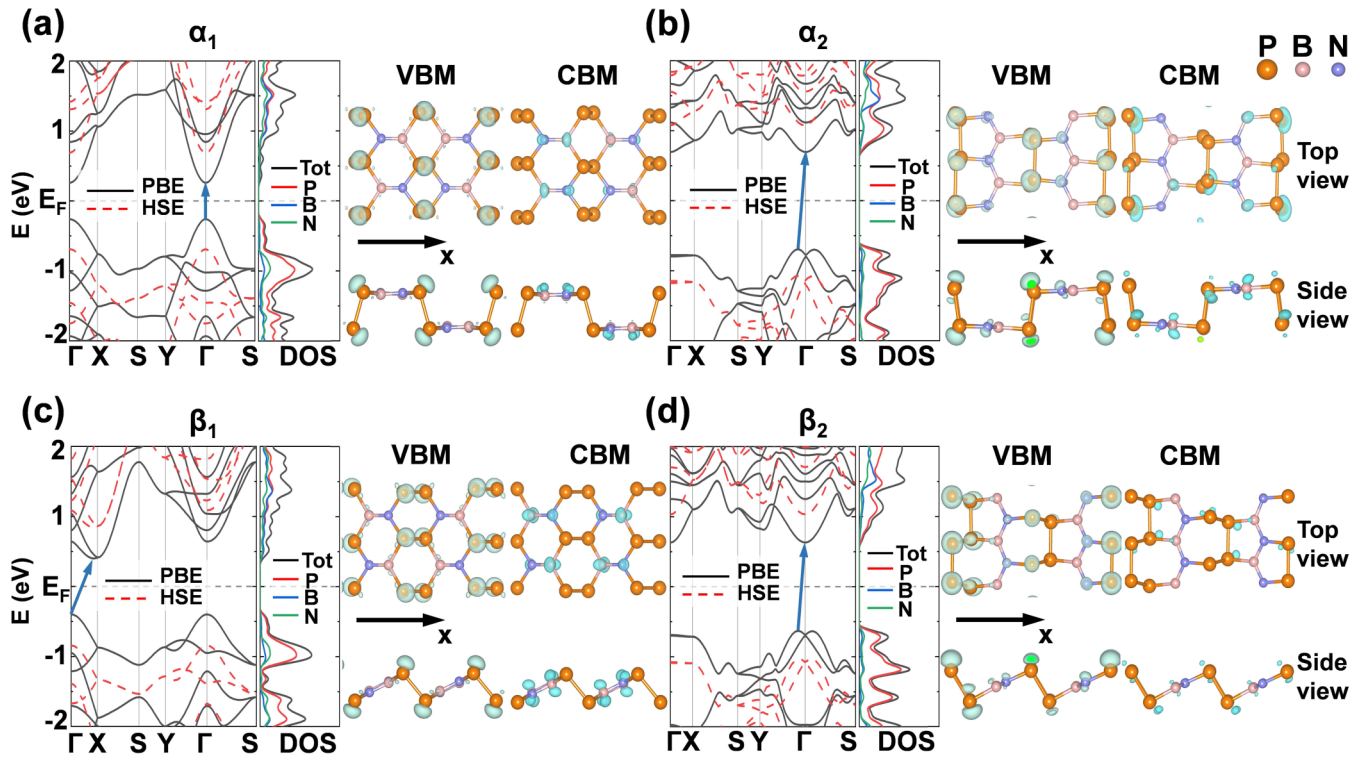
FIG. 3. Electronic structure of a BNP$_2$ monolayer. Shown are the calculated band structure $E(\mathbf{k})$ and the density of states (DOS) including its projection on individual atoms (left panels), the partial charge density distributions at the valence band maximum (VBM), and the conduction band minimum (CBM) (right panels) of the (a) α_1, (b) α_2, (c) β_1, and (d) β_2 allotropes. All results are based on the DFT-PBE functional with the exception of DFT-HSE06 data, which are shown by the red dashed lines in the band structure plots. The blue arrows indicate the fundamental band gap. Contributions of different atoms are distinguished by color in the PDOS plots. Isosurface plots of the partial charge density are presented at the isosurface value of 8.0×10^{-3} e/Bohr^3 for all allotropes.
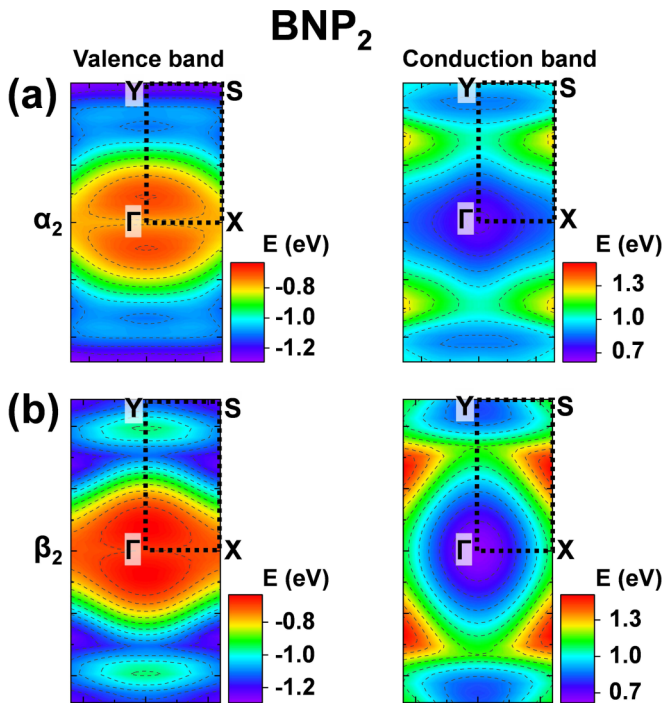

FIG. 4. Contour plots of the energy dispersion $E(\mathbf{k})$ of the top valence band (left panels) and the lowest conduction band (right panels) in (a) α_2-BNP$_2$ and (b) β_2-BNP$_2$. The Fermi level is set as the reference energy of zero.

The band gap is indirect in α_1-C$_2$SiS and direct in β_1-C$_2$SiS. Numerical band gap values based on DFT-PBE and DFT-HSE06 are listed in Table I and fall in the range of values found in BNP$_2$.

According to Fig. 5, the character of VBM and CBM states in the semiconducting allotropes α_1 and β_1 is very similar. In analogy to results for BNP$_2$, the VBM of C$_2$SiS is dominated by lone-pair orbitals of Si atoms and the CBM contains mostly out-of-local-plane p orbitals of C atoms.

The α_2 and β_2 allotropes of C$_2$SiS are found to be semimetallic by both DFT-PBE and DFT-HSE06. Dirac "cones" are seen in the band structure in Figs. 5(b) and 5(d), with the Dirac point at E_F located between Γ and Y in the Brillouin zone. The frontier states at E_F are dominated by out-of-plane p orbitals on C atoms.

The Dirac "cones" of α_2- and β_2-C$_2$SiS are visualized in more detail in Fig. 6. The band dispersion in both allotropes is linear around E_F but anisotropic. As seen in Figs. 6(c) and 6(d), the cross section of the "cone" at $E < E_F$ or $E > E_F$ is not a circle but rather an ellipse elongated in the k_x direction. The higher steepness of the band dispersion along the y direction near the Dirac point is a consequence of a stronger interaction between C2p orbitals within zigzag chains of carbons, aligned with the y direction. These C chains in α_2-C$_2$SiS and β_2-C$_2$SiS are clearly visible in Figs. 1(g) and 1(h). Otherwise, these "cones" are very similar in Dirac point location, band dispersion, and its anisotropy in both allotropes.
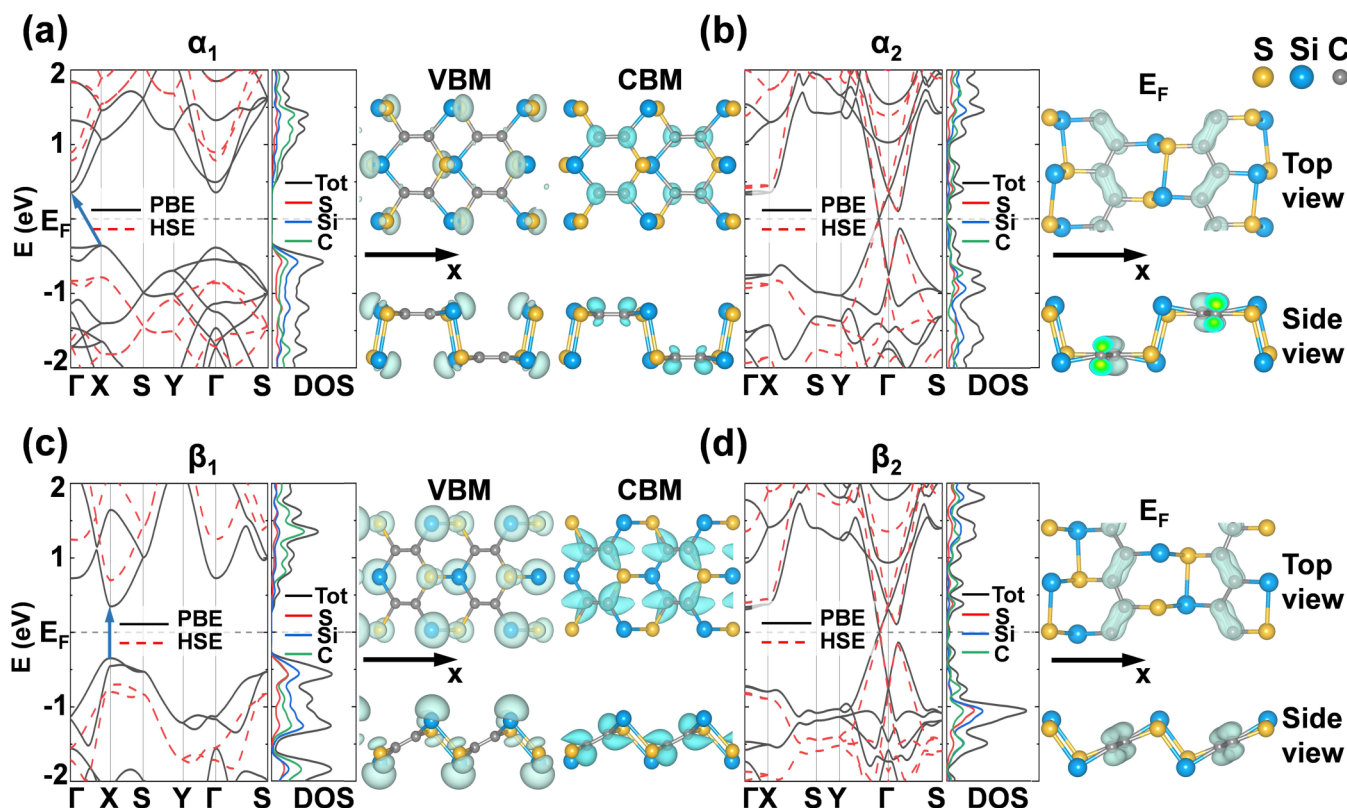
FIG. 5. Electronic structure of a C_2SiS monolayer. The calculated band structure $E(\mathbf{k})$ and the density of states (DOS) including its projection on individual atoms are shown in the left panels. The partial charge density distributions at the valence band maximum (VBM) and the conduction band minimum (CBM) for the semiconducting allotropes and for the frontier states in the semimetallic allotropes are shown in the right panels. Results are presented for the (a) α_1, (b) α_2, (c) β_1, and (d) β_2 allotropes. All results are based on the DFT-PBE functional with the exception of DFT-HSE06 data, which are shown by the red dashed lines in the band structure plots. The blue arrows indicate the fundamental band gap in the semiconducting allotropes. Contributions of different atoms are distinguished by color in the PDOS plots. Isosurface plots of the partial charge density are presented at the isosurface value of 8.0×10^{-3} e/Bohr^3 for all allotropes.

E. Carrier mobilities in semiconducting BNP_2 and C_2SiS 2D allotropes

Anisotropy in semiconducting BNP_2 and C_2SiS 2D allotropes is not only limited to the geometry, the elastic response, and the electronic structure, but is also present in the carrier mobility. In the absence of defects and external scattering centers, the mobility of carriers in 2D semiconductors is limited by acoustic phonons. We calculated the carrier mobilities of BNP_2 and C_2SiS 2D systems along the x and y direction using the deformation potential theory expression [11,44,45]

$$\mu_i = \frac{e\hbar^3 c_{ii}}{k_B T m_i^* m_d E_{1i}^2} . \qquad (2)$$

Here, i represents the Cartesian direction, with $i = 1$ standing for x and $i = 2$ for y, and e is the carrier charge. c_{ii} is the 2D elastic modulus [43] along the direction i, obtained from the strain energy curve in Fig. 2. T is the temperature, m_i^* is the effective mass along the i direction, and m_d is the average effective mass given by $m_d = (m_x^* m_y^*)^{1/2}$. The deformation potential E_{1i} along the i direction is determined at the valence band maximum (VBM) for holes and the conduction band minimum (CBM) for electrons. It is defined by $E_{1i} = \Delta V/(\Delta a_i/a_i)$, where ΔV is the energy shift of the band edge with respect to the vacuum level under a small change Δa_i of the lattice constant a_i. Our results for room-temperature carrier mobilities in all semiconducting 2D allotropes are summarized in Table II.

We found that most allotropes in our study exhibit very high and remarkably anisotropic carrier mobilities. The highest carrier mobility value we found is $\mu_y = 1.51 \times 10^5$ cm^2 V^{-1} s^{-1} for electrons in α_1-BNP_2 along the y direction, over two orders of magnitude higher than the value $\mu_x = 0.4 \times 10^3$ cm^2 V^{-1} s^{-1} along the x direction. An important contributing factor to the mobility is the 2D elastic modulus [43]. The superior electron mobility along its y direction is a result of increased stiffness along this direction. According to Table I, c_{22} is indeed much larger than c_{11} for most allotropes we study.

Unlike for electrons, hole mobility is highest along the x direction in β_1, α_2, and β_2 allotropes of BNP_2. The change of preferential transport direction is caused by substantial deformation potential anisotropy $E_{1x} < E_{1y}$ at the VBM according to Table II. Carrier mobilities in semiconducting 2D allotropes of C_2SiS are comparable to those in BNP_2.
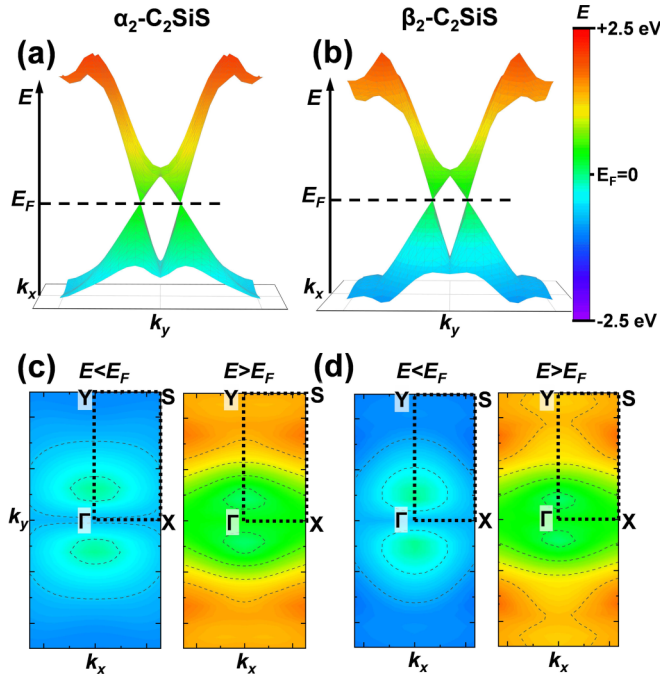
FIG. 6. Band dispersion in the semimetallic allotropes α_2-C$_2$SiS (left) and β_2-C$_2$SiS (right) near the Fermi level. $E(\mathbf{k})$ results are presented as 3D plots in (a),(b) and 2D contour plots in (c),(d). The energy with respect to $E_F = 0$ is represented by color.

Carrier mobilities $\mu > 10^5$ cm^2 V^{-1} s^{-1} in α_1-BNP$_2$ with $E_g > 0.5$ eV and $\mu \gtrsim 10^4$ cm^2 V^{-1} s^{-1} in α_2 and β_2 allotropes of BNP$_2$ with $E_g > 1$ eV, evaluated at the PBE level of DFT are unusually high in view of the wide band gaps. This is particularly evident when compared to the values found in other similar 2D materials, as discussed in the Appendix. Even though these mobilities will be reduced due to inevitable defects and the interaction with the substrate under realistic conditions, we expect values in excess of $\mu = 0.3 \times 10^3$ cm^2 V^{-1} s^{-1}, which has been reported for phosphorene [6]. These results are very promising for the realization of 2D semiconducting devices with high ON/OFF ratios and on-state currents.

IV. SUMMARY AND CONCLUSIONS

In summary, we have introduced previously unexplored 2D ternary compounds BNP$_2$ and C$_2$SiS as isoelectronic counterparts of 2D PC structures. Using *ab initio* density functional theory, we have identified four stable allotropes of each compound and confirmed their stability by calculated phonon spectra and molecular dynamics simulations. All allotropes display structural and elastic anisotropy due to structural ridges in their geometry, which are caused by coexisting sp^2 and sp^3 hybridization. Whereas all BNP$_2$ allotropes are semiconducting, we find only two allotropes of C$_2$SiS to be semiconducting. The other two allotropes of C$_2$SiS are semimetallic and show anisotropic Dirac cones at E_F. The fundamental band gaps of the semiconducting allotropes we study range from 0.5 eV to 1.4 eV at the PBE level and 1.4 eV to 2.2 eV at the HSE06 level of DFT. These 2D systems display carrier mobilities as high as 1.5×10^5 cm^2 V^{-1} s^{-1}. Such high mobilities, with two orders of magnitude in anisotropy ratio, are desirable but quite uncommon in semiconductors with so wide band gaps. Combination of wide band gaps with high and anisotropic carrier mobilities offer great promise for applications of 2D BNP$_2$ and C$_2$SiS structures in electronics and optoelectronics.

TABLE II. Calculated carrier mobilities and related quantities in semiconducting BNP$_2$ and C$_2$SiS allotropes. Electrons are denoted by e and holes by h.

		m_x^{*}[a]	m_y^{*}[a]	E_{1x}[b]	E_{1y}[b]	μ_x[c]	μ_y[c]
		(m_0)		(eV)		(10^3 cm^2 V^{-1} s^{-1})	
α_1-BNP$_2$	e	0.51	0.34	1.36	0.40	0.40	151.21
	h	0.75	0.39	1.83	1.60	0.11	6.16
β_1-BNP$_2$	e	0.67	0.34	0.69	1.37	5.89	10.51
	h	0.67	0.57	0.37	1.26	15.82	5.62
α_2-BNP$_2$	e	0.88	0.78	1.01	0.88	0.30	8.29
	h	3.13	0.50	0.10	5.07	5.67	0.26
β_2-BNP$_2$	e	0.53	0.75	2.41	0.68	0.65	17.17
	h	1.63	0.52	0.90	5.96	1.03	0.22
α_1-C$_2$SiS	e	0.53	0.28	0.39	1.37	4.38	15.66
	h	1.72	0.76	2.54	0.87	0.01	4.85
β_1-C$_2$SiS	e	0.14	1.57	2.51	6.31	1.69	0.09
	h	0.78	2.24	1.87	1.42	0.20	0.45

[a]m_x^{*} (m_y^{*}) are the carrier effective masses along the x (y) direction.

[b]E_{1x} (E_{1y}) are the deformation potentials along the x (y) direction.

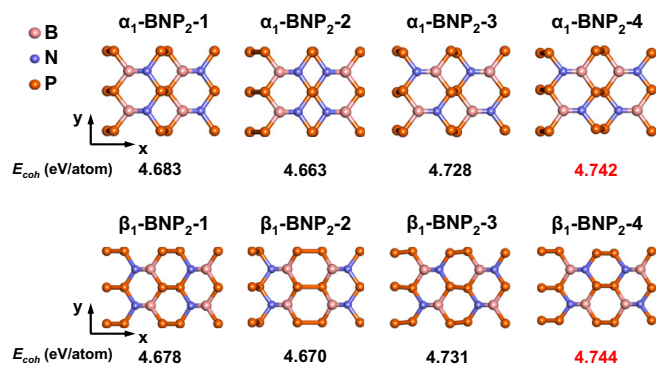[c]μ_x (μ_y) are the carrier mobilities along the x (y) direction at 300 K.

FIG. 7. Ball-and-stick model of metastable structures related to the α_1 and β_1 allotropes of BNP_2, shown in top view. Cohesive energies E_{coh} are presented below each structure, with the value for the most stable configuration highlighted in red.

APPENDIX

1. Metastable structures of 2D BNP_2 and C_2SiS

As seen in Fig. 1 of the main text, α_1 and β_1 allotropes of BNP_2 contain four polar B-N dimers aligned with the x axis in each unit cell. Each of these dimer bonds may be rotated by $180°$. This gives rise to four metastable structures for α_1-BNP_2 and another four structures for β_1-BNP_2, shown in Fig. 7. The most stable structures among these, with the cohesive energy value highlighted in red, have been considered in the main text.

Quite different is the arrangement of B and N atoms in zigzag chains in the α_2 and β_2 allotropes of BNP_2 shown in Fig. 1 of the main text. Also in this case, each bond may be rotated by $180°$. This gives rise to two metastable structures for α_2-BNP_2 and another two structures for β_2-BNP_2, shown in Fig. 8. Only the most stable among these allotropes have been considered in the main text.

Next we turn to the α_1 and β_1 allotropes of C_2SiS, displayed in Figs. 1(e) and 1(f) of the main text. Unlike in BNP_2, we can find only three inequivalent metastable structures for these systems, displayed in Fig. 9. For the α_2 and β_2 allotropes of C_2SiS, optimization leads to only one stable structure. As for the other systems discussed above, we only consider the most stable allotropes in the main text.

2. Phonon spectra of 2D BNP_2 and C_2SiS allotropes

A real confirmation of structural stability, more important than a high cohesive energy, comes from the phonon spectra. Structures can be considered stable if no imaginary frequencies can be found in the phonon spectra. The calculated phonon spectra of all BNP_2 and C_2SiS allotropes discussed in this study are displayed in Fig. 10.

We should note at this point that phonon calculations for 2D structures with the uniquely soft flexural ZA mode are very demanding on precision [46]. We found our phonon spec-
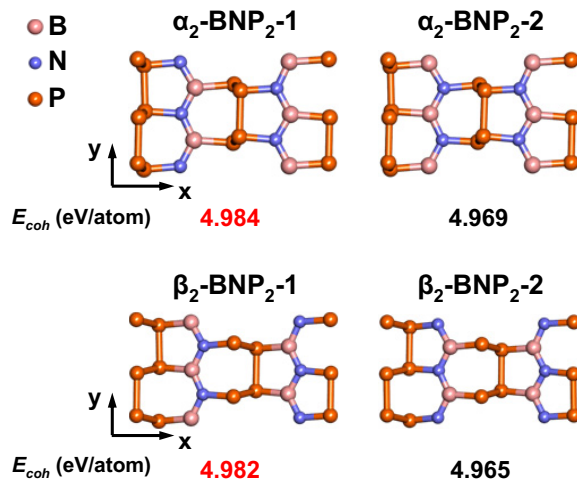
tra to be essentially free of imaginary frequencies associated with decay modes. The highest imaginary frequency value $\omega \lesssim 12i$ cm^{-1} in our spectra belongs to the ZA mode near the Γ point in the Brillouin zone and is an artifact related to numerical precision [46].

3. Thermodynamic stability of 2D BNP_2 and C_2SiS allotropes

Whereas phonon spectra tell about structural stability in the harmonic regime, they cannot determine if a structure will or will not fall apart at a given finite temperature. To study the thermodynamic stability of the ternary structures in this study, we performed a set of canonical *ab initio* molecular dynamics (MD) simulations at 300 K, 500 K, and 1000 K and present our results in Fig. 11 for 2D BNP_2 and Fig. 12 for
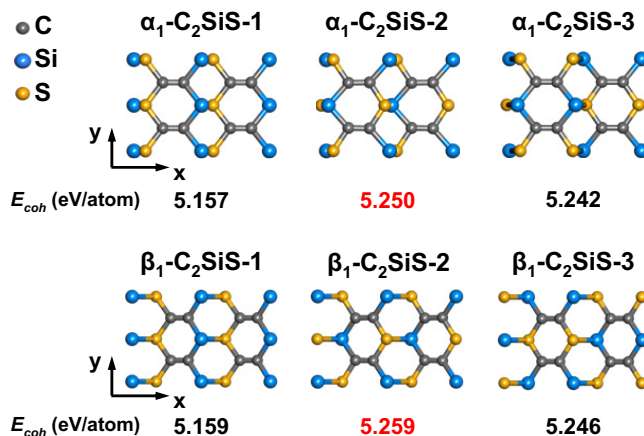

FIG. 8. Ball-and-stick model of metastable structures related to the α_1 and β_1 allotropes of C_2SiS, shown in top view. Cohesive energies E_{coh} are presented below each structure, with the value for the most stable configuration highlighted in red.

FIG. 9. Ball-and-stick model of metastable structures related to the α_2 and β_2 allotropes of BNP_2, shown in top view. Cohesive energies E_{coh} are presented below each structure, with the value for the most stable configuration highlighted in red.
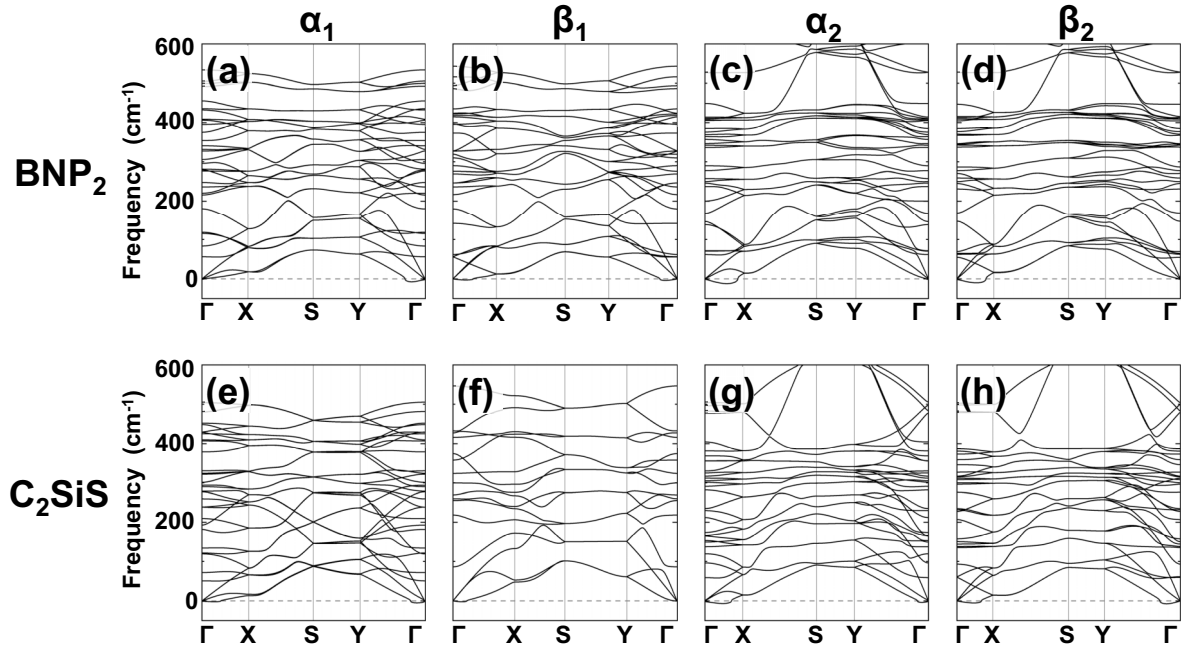
FIG. 10. Phonon spectra for monolayers of (a) α_1-BNP$_2$, (b) β_1-BNP$_2$, (c) α_2-BNP$_2$, (d) β_2-BNP$_2$, (e) α_1-C$_2$SiS, (f) β_1-C$_2$SiS, (g) α_2-C$_2$SiS, and (h) β_2-C$_2$SiS.

C$_2$SiS structures. For 15 ps long MD runs, we plotted both the fluctuations of the total potential energy and snapshots of the structures after 15 ps.

Our results in Fig. 11 indicate that all four allotropes of BNP$_2$ maintained their geometries up to 1000 K, indicating a high thermodynamic stability. The corresponding results

FIG. 11. Fluctuations of the total potential energy (left panels) and structural snap shots after 15 ps (right panels) for (a) α_1-BNP$_2$, (b) α_2-BNP$_2$, (c) β_1-BNP$_2$, and (d) β_2-BNP$_2$ monolayers during canonical MD simulations at 300 K, 500 K, and 1000 K.
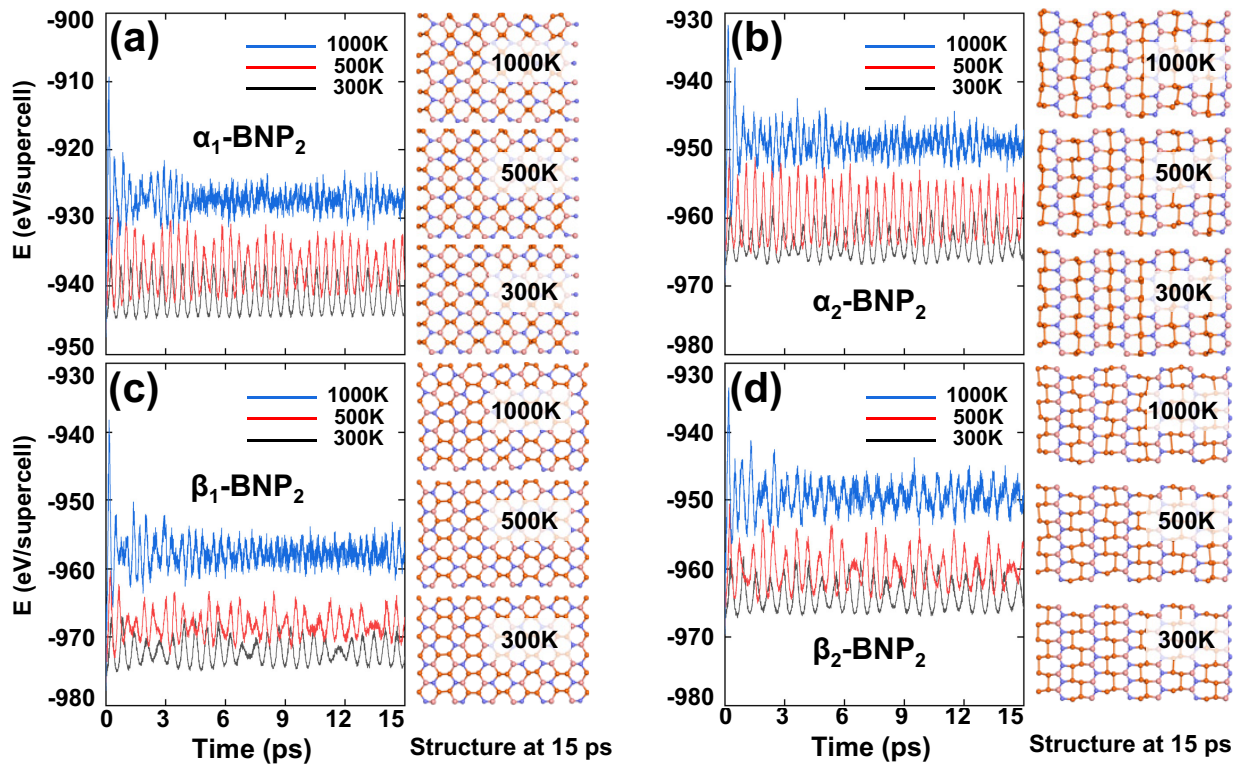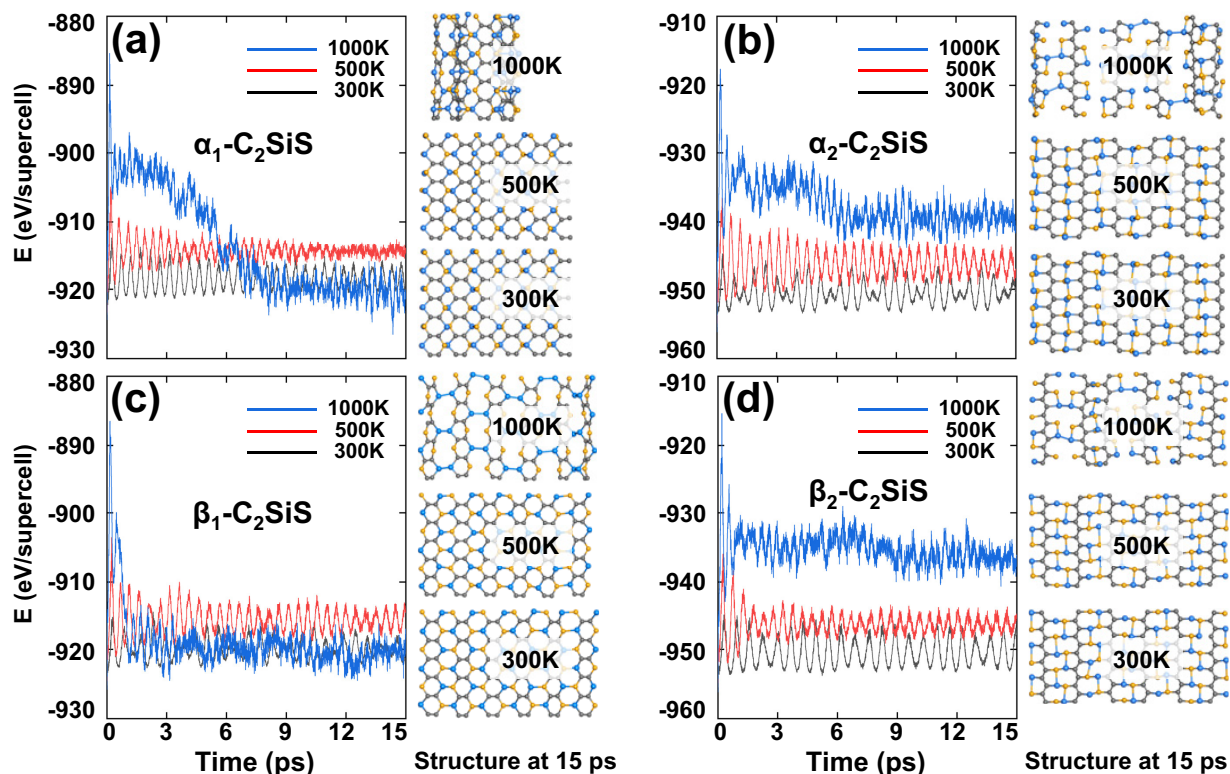
FIG. 12. Fluctuations of the total potential energy (left panels) and structural snap shots after 15 ps (right panels) for (a) α_1-C_2SiS, (b) α_2-C_2SiS, (c) β_1-C_2SiS, and (d) β_2-C_2SiS monolayers during canonical MD simulations at 300 K, 500 K, and 1000 K.

for C_2SiS in Fig. 12 indicate all allotropes to be stable at 300 K and 500 K. Further increase of temperature to 1000 K causes a dramatic degradation of the α_1 and β_1 allotropes of
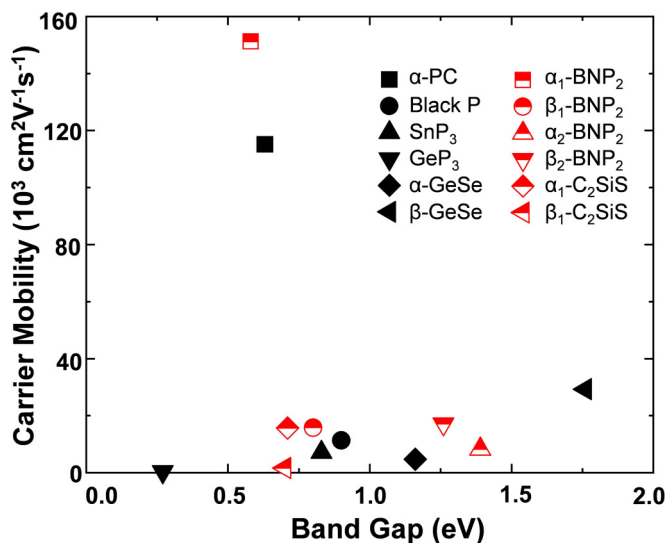

FIG. 13. Carrier mobility versus band gap for different 2D materials. Results for semiconducting allotropes predicted in this study, shown by the red symbols, are compared to previously reported results, cited in the text tand shown by the black symbols. All results have been obtained at the PBE level of DFT.

C_2SiS after 3 ps. The α_2 and β_2 allotropes appear more stable at 1000 K, but their significant distortion indicates onset of degradation. The thermodynamic stability of all the BNP_2 and C_2SiS allotropes is either comparable to or superior to other similar 2D structures including GeP_3 [16], which was shown to be stable at $T \lesssim 500$ K, as well as PC [11] and binary V-V compounds [47], which were shown to be stable only up to ≈ 300 K. Our MD results show good consistency with the conclusions obtained from the formation energy calculations discussed in the main text.

4. Suitability of BNP_2 and C_2SiS allotropes for electronic applications

Combination of high carrier mobility and wide band gap is very desirable, as it results in a high ON/OFF ratio and a high on-state current in semiconductor devices. The 2D materials we introduce appear particularly suitable for electronic applications from that viewpoint. This is evidenced in Fig. 13, where we compare mobilities and band gaps of BNP_2 and C_2SiS to those of 2D-PC [10], GeP_3 [16], SnP_3 [17], black phosphorene, and 2D GeSe [48]. There is a general tradeoff relation between carrier mobility and band gap. We find most of the BNP_2 and C_2SiS allotropes to be near the upper limit of the tradeoff.

 [1] K. S. Novoselov, A. K. Geim, S. V. Morozov, D. Jiang, Y. Zhang, S. V. Dubonos, I. V. Grigorieva, and A. A. Firsov, Electric field effect in atomically thin carbon films, Science **306**, 666 (2004).

 [2] K. S. Novoselov, A. K. Geim, S. V. Morozov, D. Jiang, M. I. Katsnelson, I. V. Grigorieva, S. V. Dubonos, and A. A. Firsov, Two-dimensional gas of massless Dirac fermions in graphene, Nature (London) **438**, 197 (2005).

 [3] Y. Zhang, Y.-W. Tan, H. L. Stormer, and P. Kim, Experimental observation of the quantum Hall effect and Berry's phase in graphene, Nature (London) **438**, 201 (2005).

 [4] B. Radisavljevic, A. Radenovic, J. Brivio, V. Giacometti, and A. Kis, Single-layer MoS$_2$ transistors, Nat. Nanotechnol. **6**, 147 (2011).

 [5] M. S. Fuhrer and J. Hone, Measurement of mobility in dual-gated MoS$_2$ transistors, Nat. Nanotechnol. **8**, 146 (2013).

 [6] H. Liu, A. T. Neal, Z. Zhu, Z. Luo, X. Xu, D. Tománek, and P. D. Ye, Phosphorene: An unexplored 2D semiconductor with a high hole mobility, ACS Nano **8**, 4033 (2014).

 [7] L. Li, Y. Yu, G. J. Ye, Q. Ge, X. Ou, H. Wu, D. Feng, X. H. Chen, and Y. Zhang, Black phosphorus field-effect transistors, Nat. Nanotechnol. **9**, 372 (2014).

 [8] L. Wang, A. Kutana, X. Zou, and B. I. Yakobson, Electromechanical anisotropy of phosphorene, Nanoscale **7**, 9746 (2015).

 [9] J. D. Wood, S. A. Wells, D. Jariwala, K.-S. Chen, E. Cho, V. K. Sangwan, X. Liu, L. J. Lauhon, T. J. Marks, and M. C. Hersam, Effective passivation of exfoliated black phosphorus transistors against ambient degradation, Nano Lett. **14**, 6964 (2014).

[10] J. Guan, D. Liu, Z. Zhu, and D. Tománek, Two-dimensional phosphorus carbide: Competition between sp^2 and sp^3 bonding, Nano Lett. **16**, 3247 (2016).

[11] G. Wang, R. Pandey, and S. P. Karna, Carbon phosphide monolayers with superior carrier mobility, Nanoscale **8**, 8819 (2016).

[12] W. C. Tan, Y. Cai, R. J. Ng, L. Huang, X. Feng, G. Zhang, Y.-W. Zhang, C. A. Nijhuis, X. Liu, and K.-W. Ang, Few-layer black phosphorus carbide field-effect transistor via carbon doping, Adv. Mater. **29**, 1700503 (2017).

[13] W. C. Tan, L. Huang, R. J. Ng, L. Wang, D. M. N. Hasan, T. J. Duffin, K. S. Kumar, C. A. Nijhuis, C. Lee, and K.-W. Ang, A black phosphorus carbide infrared phototransistor, Adv. Mater. **30**, 1705039 (2018).

[14] X. Huang, Y. Cai, X. Feng, W. C. Tan, D. M. N. Hasan, L. Chen, N. Chen, L. Wang, L. Huang, T. J. Duffin, C. A. Nijhuis, Y.-W. Zhang, C. Lee, and K.-W. Ang, Black phosphorus carbide as a tunable anisotropic plasmonic metasurface, ACS Photon. **5**, 3116 (2018).

[15] L. Li, W. Wang, P. Gong, X. Zhu, B. Deng, X. Shi, G. Gao, H. Li, and T. Zhai, 2D GeP: An unexploited low-symmetry semiconductor with strong in-plane anisotropy, Adv. Mater. **30**, 1706771 (2018).

[16] Y. Jing, Y. Ma, Y. Li, and T. Heine, GeP$_3$: A small indirect band gap 2D crystal with high carrier mobility and strong interlayer quantum confinement, Nano Lett. **17**, 1833 (2017).

[17] B. Ghosh, S. Puri, A. Agarwal, and S. Bhowmick, SnP$_3$: A previously unexplored two-dimensional material, J. Phys. Chem. C **122**, 18185 (2018).

[18] T. Yu, Z. Zhao, Y. Sun, A. Bergara, J. Lin, S. Zhang, H. Xu, L. Zhang, G. Yang, and Y. Liu, Two-dimensional PC$_6$ with direct band gap and anisotropic carrier mobility, J. Am. Chem. Soc. **141**, 1599 (2019).

[19] J.-H. Yang, Y. Zhai, H. Liu, H. Xiang, X. Gong, and S.-H. Wei, Si$_3$AlP: A new promising material for solar cell absorber, J. Am. Chem. Soc. **134**, 12653 (2012).

[20] Z. Zhu, J. Guan, D. Liu, and D. Tománek, Designing isoelectronic counterparts to layered group V semiconductors, ACS Nano **9**, 8284 (2015).

[21] J.-H. Yang, Y. Zhang, W.-J. Yin, X. G. Gong, B. I. Yakobson, and S.-H. Wei, Two-dimensional SiS layers with promising electronic and optoelectronic properties: Theoretical prediction, Nano Lett. **16**, 1110 (2016).

[22] L. C. Gomes and A. Carvalho, Phosphorene analogues: Isoelectronic two-dimensional group-IV monochalcogenides with orthorhombic structure, Phys. Rev. B **92**, 085406 (2015).

[23] L. C. Gomes, A. Carvalho, and A. H. Castro Neto, Enhanced piezoelectricity and modified dielectric screening of two-dimensional group-IV monochalcogenides, Phys. Rev. B **92**, 214103 (2015).

[24] R. Fei, W. Kang, and L. Yang, Ferroelectricity and Phase Transitions in Monolayer Group-IV Monochalcogenides, Phys. Rev. Lett. **117**, 097601 (2016).

[25] R. Haleoot, C. Paillard, T. P. Kaloni, M. Mehboudi, B. Xu, L. Bellaiche, and S. Barraza-Lopez, Photostrictive Two-Dimensional Materials in the Monochalcogenide Family, Phys. Rev. Lett. **118**, 227401 (2017).

[26] G. Kresse and J. Furthmüller, Efficient iterative schemes for *ab initio* total-energy calculations using a plane-wave basis set, Phys. Rev. B **54**, 11169 (1996).

[27] G. Kresse and J. Hafner, *Ab initio* molecular dynamics for liquid metals, Phys. Rev. B **47**, 558 (1993).

[28] G. Kresse and J. Hafner, *Ab initio* molecular-dynamics simulation of the liquid-metal–amorphous-semiconductor transition in germanium, Phys. Rev. B **49**, 14251 (1994).

[29] H. J. Monkhorst and J. D. Pack, Special points for Brillouin-zone integrations, Phys. Rev. B **13**, 5188 (1976).

[30] G. Kresse and D. Joubert, From ultrasoft pseudopotentials to the projector augmented-wave method, Phys. Rev. B **59**, 1758 (1999).

[31] J. P. Perdew, K. Burke, and M. Ernzerhof, Generalized Gradient Approximation Made Simple, Phys. Rev. Lett. **77**, 3865 (1996).

[32] J. Heyd, G. E. Scuseria, and M. Ernzerhof, Hybrid functionals based on a screened Coulomb potential, J. Chem. Phys. **118**, 8207 (2003).

[33] J. Heyd, G. E. Scuseria, and M. Ernzerhof, Erratum: "Hybrid functionals based on a screened Coulomb potential" [J. Chem. Phys. 118, 8207 (2003)], J. Chem. Phys. **124**, 219906 (2006).

[34] S. Grimme, Semiempirical GGA-type density functional constructed with a long-range dispersion correction, J. Comp. Chem. **27**, 1787 (2006).

[35] M. R. Hestenes and E. Stiefel, Methods of conjugate gradients for solving linear systems, J. Res. Natl. Bur. Stand. **49**, 409 (1952).

[36] S. Baroni, P. Giannozzi, and A. Testa, Green's-Function Approach to Linear Response in Solids, Phys. Rev. Lett. **58**, 1861 (1987).

[37] X. Gonze, Adiabatic density-functional perturbation theory, Phys. Rev. A **52**, 1096 (1995).

[38] X. Gonze, Perturbation expansion of variational principles at arbitrary order, Phys. Rev. A **52**, 1086 (1995).

[39] A. Togo and I. Tanaka, First principles phonon calculations in materials science, Scr. Mater. **108**, 1 (2015).

[40] Z. Zhu and D. Tománek, Semiconducting Layered Blue Phosphorus: A Computational Study, Phys. Rev. Lett. **112**, 176802 (2014).

[41] M. Sugie, H. Takeo, and C. Matsumura, Microwave spectrum of aminoborane, BH_2NH_2, Chem. Phys. Lett. **64**, 573 (1979).

[42] H. Şahin, S. Cahangirov, M. Topsakal, E. Bekaroglu, E. Akturk, R. T. Senger, and S. Ciraci, Monolayer honeycomb structures of group-IV elements and III-V binary compounds: First-principles calculations, Phys. Rev. B **80**, 155453 (2009).

[43] D. Liu, A. G. Every, and D. Tománek, Continuum approach for long-wavelength acoustic phonons in quasi-two-dimensional structures, Phys. Rev. B **94**, 165432 (2016).

[44] J. Bardeen and W. Shockley, Deformation potentials and mobilities in non-polar crystals, Phys. Rev. **80**, 72 (1950).

[45] J. Qiao, X. Kong, Z.-X. Hu, F. Yang, and W. Ji, High-mobility transport anisotropy and linear dichroism in few-layer black phosphorus, Nat. Commun. **5**, 4475 (2014).

[46] V. Zólyomi, N. D. Drummond, and V. I. Fal'ko, Electrons and phonons in single layers of hexagonal indium chalcogenides from *ab initio* calculations, Phys. Rev. B **89**, 205416 (2014).

[47] W. Yu, C.-Y. Niu, Z. Zhu, X. Wang, and W.-B. Zhang, Atomically thin binary V-V compound semiconductor: A first-principles study, J. Mater. Chem. C **4**, 6581 (2016).

[48] Y. Xu, H. Zhang, H. Shao, G. Ni, J. Li, H. Lu, R. Zhang, B. Peng, Y. Zhu, H. Zhu, and C. M. Soukoulis, First-principles study on the electronic, optical, and transport properties of monolayer α- and β-GeSe, Phys. Rev. B **96**, 245421 (2017).